2014

High-performance sodium-ion batteries and sodium-ion pseudocapacitors based on MoS2/graphene composites

Yunxiao Wang
University of Wollongong, yw708@uowmail.edu.au

Shulei Chou
University of Wollongong, shulei@uow.edu.au

David Wexler
University of Wollongong, davidw@uow.edu.au

Hua-Kun Liu
University of Wollongong, hua@uow.edu.au

S X. Dou
University of Wollongong, shi@uow.edu.au

Publication Details

Wang, Y., Chou, S., Wexler, D., Liu, H. & Dou, S. (2014). High-performance sodium-ion batteries and sodium-ion pseudocapacitors based on MoS2/graphene composites. Chemistry: A European Journal, 20 (31), 9607-9612.

High-performance sodium-ion batteries and sodium-ion pseudocapacitors based on MoS2/graphene composites

Abstract

Sodium-ion energy storage, including sodium-ion batteries (NIBs) and electrochemical capacitive storage (NICs), is considered as a promising alternative to lithium-ion energy storage. It is an intriguing prospect, especially for large-scale applications, owing to its low cost and abundance. MoS2 sodiation/desodiation with Na ions is based on the conversion reaction, which is not only able to deliver higher capacity than the intercalation reaction, but can also be applied in capacitive storage owing to its typically sloping charge/discharge curves. Here, NIBs and NICs based on a graphene composite (MoS2/G) were constructed. The enlarged d-spacing, a contribution of the graphene matrix, and the unique properties of the MoS2/G substantially optimize Na storage behavior, by accommodating large volume changes and facilitating fast ion diffusion. MoS2/G exhibits a stable capacity of approximately 350 mAh g−1 over 200 cycles at 0.25 C in half cells, and delivers a capacitance of 50 F g−1 over 2000 cycles at 1.5 C in pseudocapacitors with a wide voltage window of 0.1-2.5 V.

Keywords

batteries, performance, pseudocapacitors, mos2, graphene, composites, sodium, ion, high

Disciplines

Engineering | Physical Sciences and Mathematics

Publication Details

Wang, Y., Chou, S., Wexler, D., Liu, H. & Dou, S. (2014). High-performance sodium-ion batteries and sodium-ion pseudocapacitors based on MoS2/graphene composites. Chemistry: A European Journal, 20 (31), 9607-9612.

High-Performance Sodium-Ion Batteries and Sodium-Ion Pseudocapacitors Based On MoS_2/Graphene Composites

Abstract: Sodium-ion energy storage, including sodium-ion batteries (NIBs) and electrochemical capacitive storage (NICs), is considered as a promising alternative of lithium-ion energy storage. It is an intriguing prospect, especially for large-scale applications, due to its low cost and abundance. MoS_2 sodiation/desodiation with Na ions is based on the conversion reaction, which is not only able to deliver higher capacity than intercalation reaction, but is also supposed to be applied in capacitive storage due to its typically sloping harge/discharge curves. Here we construct NIBs and NICs based on graphene composite (MoS_2/G). The enlarged d-spacing, participant of graphene matrix, and the unique properties of the MoS_2/G substantially optimize Na storage behaviors, accommodating large volume changes and facilitating fast ion diffusion as well. MoS_2/G can exhibit a stable capacity of ~350 mAh g^{-1} over 200 cycles at 0.25 C in half cells, and delivers a capacitance of 50 F g^{-1} over 2000 cycles at 1.5 C in pseudocapacitors with a wide voltage window of 0.1-2.5 V.

Yun-Xiao Wang, Shu-Lei Chou,* David Wexler, Hua-Kun Liu, and Shi-Xue Dou

Introduction

Considering current rechargeable battery systems for renewable energy storage, lead acid, nickel/cadmium, and vanadium-redox flow batteries all suffer from serious environmental problems; use of sodium/sulphur battery is limited because of the high operating temperature (~350 ^{o}C); rechargeable lithium-ion batteries (LIBs), as the mainstay of energy storage, have been successfully commercialized in portable electronic devices.[1,2] LIBs, however, are encountering an inevitable challenge with respect to large-scale energy storage due to both lithium resources and cost. Thus, it is significant and urgent to develop an essentially new battery system, which needs to be low cost, environmentally friendly, and safe. Sodium, located in the same main group in the periodic table after lithium, is one of the most attractive elements to replace lithium. It is 4-5 orders of magnitude more abundant than lithium, and the cost of the sodium-based materials is much lower than for the lithium-based materials. In addition, the standard potential of Na^+/Na (-2. 71 V) is slightly higher than that of Li^+/Li (-3.05 V). These features point to the great potential of sodium-ion batteries for renewable energy and smart grids.[3,4] To date, various cathode materials, including layered transition metal oxides,[5-8]organic polymers,[3,9,10] and polyanion fluorophosphates,[11-15] have been reported to reversibly accommodate Na ions. Anode research is mainly focused on carbonaceous material,[16-18] alloyable metals,[19] alloyable metal oxides/sulfides[20-23] and non-metal elements.[24,25] Furthermore, electrochemical capacitors are receiving great attention as well, because of their significantly higher power density than batteries with prolonged cycle life, although they also have relatively lower energy density than batteries.[26,27] To combine the advantages of both batteries and capacitors, Na-based electrochemical capacitors have been proposed and are also a fascinating alternative for future energy storage.[28,29]

Molybdenum disulphide (MoS_2), with an analogous structure to graphite, possesses S-Mo-S sandwich layered structure, Specifically, atoms within the layers of MoS_2 are bound by strong covalent bonds, whereas the individual layers are bound together by weak van der Waals interactions. Many reports have involved the application of MoS_2 in lithium-ion batteries, since lithium ions can intercalate between the layers.[30-32] Remarkably, expanded MoS_2, fabricated via lithiation method with an enlarged c lattice parameter, has achieved higher capacity with longer cycling span than commercial MoS_2 (C-MoS_2). The expanded MoS_2 tends to be prone to serious restacking, however, due to its high surface energy. Moreover, the poor electronic/ionic conductivity between adjacent S-Mo-S sheets further obstructs its application as electrode material. Thus, many researchers have turned to assembling graphene sheets with expanded MoS_2 to construct three-dimensional (3D) architectures. The obtained MoS_2/G composite would offer high specific surface area, strong mechanical strength, and fast mass transport kinetics. More importantly, the graphene matrix can not only effectively enhance the conductivity and stability of the active materials, but also can significantly inhibit the aggregation of exfoliated MoS_2 sheets. The reported studies show that MoS_2/G composite possesses synergistic effects between the layered MoS_2 and the graphene, which result in good electrochemical properties in LIBs.[33,34] This strategy is capable of capitalizing on the advantages of MoS_2

Y.-X. Wang, Dr. S.-L. Chou, D. Wexler, Prof. H.-K. Liu, Prof. S.-X. Dou,
Institute for Superconducting & Electronic Materials (ISEM), Innovation Campus, University of Wollongong, Wollongong, NSW, 2519, Australia.
E-mail: shulei@uow.edu.au

Supporting information for this article is available on the WWW under http://dx.doi.org/10.1002/cssc.20xxxxxxx.

anode. Recently, the research on MoS_2 has been extended to the sodium-ion battery, and the intercalation mechanism of MoS_2 and Na has been confirmed over the narrow voltage range of 0.4-2.6 V, with the electrode delivering a low capacity of 85 mAh g^{-1} over 100 cycles.[35] The most recently, Singh's group explored the electrochemical performance of free-standing MoS_2/G composite paper. However, the best electrode with 73 wt. % MoS_2 in the composite only delivers a low capacity of 218 mAh g^{-1} after 20 cycles.[36]

Herein, we report that expanded MoS_2/G composite (MoS_2/G), which was prepared by the attachment of expanded MoS_2 layers onto graphene sheets by a simple hydrothermal method, results in excellent electrochemical properties in both the sodium ion battery and the sodium-ion pseudocapacitor. The sodium ion battery is able to deliver a high capacity of 313 mAh g^{-1} over 200 cycles at 0.25 C (1 C= 400 mA g^{-1}), with capacity retention of 81%. As for the sodium ion pseudocapacitor, the sodium-ion capacitor (NIC) full cell shows excellent cycling performance over 2000 cycles with relatively stable capacitance (~50 F g^{-1}) at 1.5 C. Hence, MoS_2/G can achieve good energy and power density, high rate capability, and good cycling stability in Na-ion electrodes and pseudocapacitors, providing a promising candidate for high-performance and sustainable energy storage systems.

Results and Discussions

As shown by the schematic illustration in Figure 1a, in spite of the large lattice mismatch between expanded MoS_2 and graphene, the MoS_2 layers are attached to the graphene sheets matrix, presumably via van der Waals interactions. Besides the unique properties mentioned above, more interestingly, the MoS_2/G interfaces show intriguing phenomenon according to *ab initio* calculations,[37] which indicates an energetic preference for Li atom intercalation (MoS_2/Li/G), in comparison with Li atoms on the MoS_2 surface (Li/MoS_2 and Li/MoS_2/G), thus leading to higher Li storage capacity in the MoS_2/G composite. It is reasonable that the MoS_2/G interface is able to facilitate the accommodation of Na ions, exhibiting higher capacity than MoS_2. It can be seen that G, expanded MoS_2 and MoS_2/G composite show similar layered

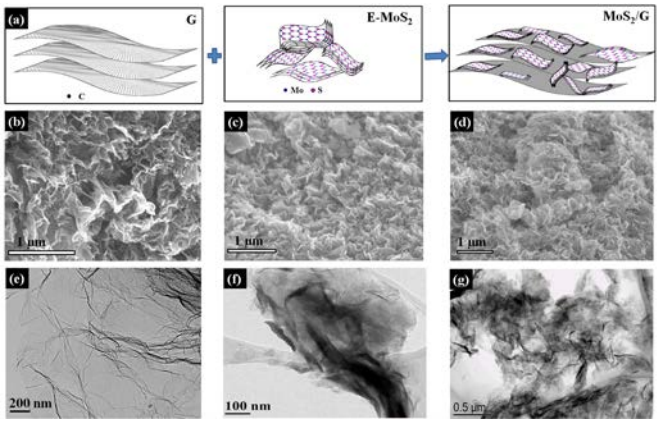

Figure 1. Morphologies of graphene, E-MoS_2 and MoS_2/G composite: (a), Schematic illustrations of the synthesis of MoS_2/G composite; (b), (c), (d), SEM micrographs; (e), (f), (g), TEM micrographs of graphene, expanded MoS_2 and MoS_2/G composite.

structures, and no significant morphological changes observed between MoS_2 and MoS_2/G composite. As shown in Figure 1b, the graphene sheets overlap each other with a crumpled structure, which allows plenty of free room between the graphene layers. The free room can accommodate the adherence of MoS_2 layers. Furthermore, the obtained graphene nanosheets are very thin and have a large size, as shown in Figure 1e, which implies that the graphene nanosheets are only stacked in a few layers and allow MoS_2 layers to be quite uniformly dispersed on their surface. Elemental mapping (Fig. S1 in the supporting information) verify the even dispersion of MoS_2 layers on a graphene matrix. As can be seen in Figure 1c, there are small MoS_2 bulks in the expanded MoS_2 (E-MoS_2), which is ascribed to the restacking/agglomeration effect of the exfoliated MoS_2 layers. In contrast, the MoS_2/G shown in Figure 1d has a much looser packing of nanosheets and presents a more transparent appearance. The TEM images in Figure 1f and g further confirm that the MoS_2 layers intend to adhere to the graphene sheets, hindering the restacking of exfoliated MoS_2. The physical characteristics of C-MoS_2, E-MoS_2, and MoS_2/G were further observed by X-ray diffraction (XRD) analysis and high resolution transmission electron microscopy (HRTEM), respectively. The results in Supplementary Fig.S2 reveal that the incorporation of graphene can effectively inhibit the restacking/agglomeration of E-MoS_2 layers. In addition, it is noteworthy that the (002) diffraction peak of G cannot be detected in MoS_2/G, indicating that the graphene layers are separated by MoS_2 layers in the composite. Raman spectrum of MoS_2/G (Supplementary Fig.S3) presents the D-bond and G-bond of G at 1342 and 1593 cm^{-1}, respectively, confirming the presence of G in the composite. Thermogravimetric analysis (TGA) (Supplementary Fig.S4) was carried out to measure the ratio MoS_2 to graphene, which is calculated to be ~77 wt. % of MoS_2 in the composite.

In order to evaluate the sodium-ion storage properties of MoS_2/G, the electrochemical performances of sodium ion half-cell and pseudocapacitor were tested, respectively. As shown in Figure 2a, the half-cell is composed of MoS_2/G anode and Na plate separated by glass fiber separators. In contrast to C-MoS2,

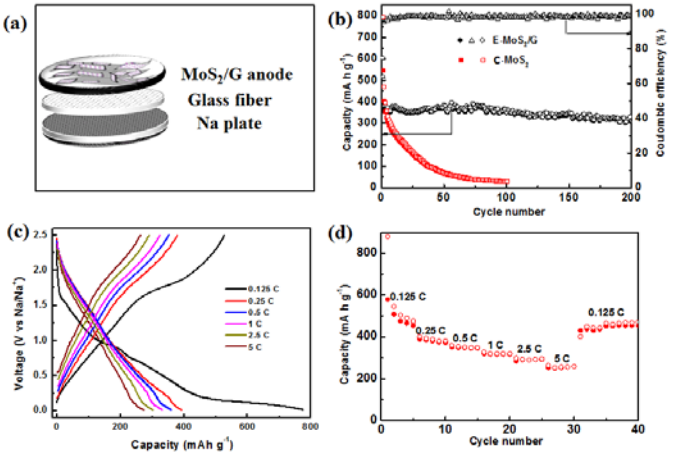

Figure 2. Electrochemical performances of half cells: (a) schematic structure of sodium-ion battery; (b) cycling performances of C-MoS_2 and MoS_2/G composite at 100 mA g^{-1} (0.25 C); and coulombic efficiency of MoS_2/G composite; (c) charge/discharge curves and (d) rate capability of MoS_2/G at various current rate.

MoS_2/G shows a dramatic enhancement on electrochemical performance (Fig. 2b), delivering a much better cycling stability

and capacity retention of 81 % over 200 cycles at 100 mA g^{-1} (0.25 C). The initial charge/discharge capacity is 386.0 and 604.3 mAh g^{-1}, respectively; the low Coulombic efficiency (~65 %) is mainly ascribed to the formation of solid electrolyte interphase (SEI) and the occurrence of irreversible reactions. The coulombic efficiency maintains above 97 %, implying that the mechanism acting in first cycle is possibly different from that in the subsequent cycles. Furthermore, excellent rate capability is achieved as shown in Figure 2c and d. It was tested at different current rate of 0.125, 0.25, 0.5, 1, 2.5, and 5 C, with the capacity corresponding to 491.7, 355.6, 327.8, 302.8, 280.6, and 247.2 mAh g^{-1}, respectively. Along with the increase in the current rate, interestingly, the charge/discharge curves show more obvious capacitive characteristics, with sloping curves and large voltage hysteresis. Thus, we can speculate that it is feasible to apply MoS_2/G in a capacitor system. The charge/discharge curves for the first discharge process show inconspicuous plateaus during 1.7 - 0.5 V, which disappears from the second cycle, indicating a different mechanism in the following cycles. An obvious long plateau at about 0.3 V is observed, which implies that the reaction in this step is partially reversible in subsequent cycles. During the charge process, a conspicuous plateau occurs at about 1.85 V, which is corresponding to the redox reaction.

A Na-ion pseudocapacitor was constructed and examined. As shown in Figure 3a, the electrodes were sodium-doped MoS_2/G (Na_nMoS_2/G), which was prepared by galvanostatically discharging the half-cell from open circuit potential (OCP) to 0.01 V. Na ions were accommodated in the MoS_2 by the pre-sodiation process, which transformed MoS_2 into amorphous Na_nMoS_2. After disassembling two half-cells, the sodium-ion pseudocapacitor was reassembled into a coin-cell containing 1M $NaClO_4$ in propylene carbonate (PC) / ethylene carbonate (EC) + fluoroethylene carbonate (FEC) electrolyte, along with Na_nMoS_2/G positive and negative electrodes. The specific capacitance (C_m) of such full cell can be calculated by the following formula: $C_m = Q/\Delta V \times 3.6$, where Q (mAh g^{-1} a represents the specific capacity, and ΔV (V) is the charge/discharge voltage variation (excluding the IR drop). As shown in Figure 3b, the NIC full cell showed excellent cycling performance over 2000 cycles with relatively stable capacitance (~50 F g^{-1}) at 1.5 C. The charge/discharge curves are shown in Figure 3c for different current rates. With increasing current rate from 50 to 1200 mA g^{-1}, the specific capacitance decreases from 250 to 45 F g^{-1}. It is noteworthy that the initial irreversible capacity is very high, which results from the irreversibility of the intercalation reaction of first cycle. Meanwhile, the NIC with MoS_2/G and MoS_2/G electrodes was tested in comparison as shown in Figure 3d , which delivered a very low capacitance (5-15 F g^{-1}), similar to the energy density of electric double layer capacitors (EDLCs). It implies that only a non-faradic reaction takes place in this capacitor. It is obvious that Na_nMoS_2/G NIC exhibits significantly higher capacitance than that of MoS_2/G, which arises from the occurrence of the faradic reaction in the Na_nMoS_2/G NIC.

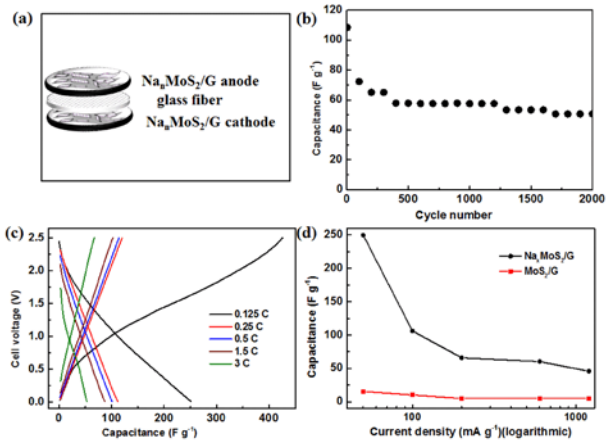

Figure 3. Electrochemical performances of full cells**:** (a) schematic structure of sodium-ion pseudocapacitor; (b) capacitance of NICs at 1.5 C with prolonged cycling; (c) charge/discharge curves of NICs at various current rates; (d) comparison of capacitance between MoS_2 NICs and Na_nMoS_2 NICs at various current rates

The Na-storage mechanism was deduced in details by ex-situ XRD of C-MoS_2, based on its good crystallization and high intensity diffraction peaks. As shown in Figure 4a, C-MoS_2 shows similar charge/discharge curves to MoS_2/G (Fig.3c), demonstrating that they are likely to be subject to the same mechanism. In addition, two pronounced plateaus at ~0.9 and ~0.75 V are observed in the first discharge profile, which is due to the ordered stacking of its layered structure and good crystallization. Powder samples of ex-situ XRD were collected by shaving off the electrode materials from the Cu current collectors under the respective corresponding conditions. Ex-situ XRD was conducted at five different states of charge and discharge as presented in Figure 4b and c. When discharged to 0.9 V, corresponding to the end of the first plateau, the (002) diffraction peak shows a slight shift towards lower angle. This indicates expansion of the interlayer spacing between the (002) planes due to Na ion intercalation into the layer sites of MoS_2. The specific capacity recorded at the end of this plateau was 84 mAh g^{-1}, which can be related to the formation of $Na_{0.5}MoS_2$. When the electrodes are discharged to 0.75 V, the diffraction peaks of 2H-MoS_2 are no longer observed. Two diffraction peaks appear at 9.54° and 19.8°, which are indexed to $NaMoS_2$ (JCPDS Card No. 18-1257). The capacity recorded after the second plateau is 175mAh g^{-1}, which is similar to the theoretical capacity of one Na^+ intercalation (167 mAh g^{-1}), confirming the formation of $NaMoS_2$. When fully discharged to 0.01 V, no obvious peaks can be observed, apart from two broadened peaks, which indicates the

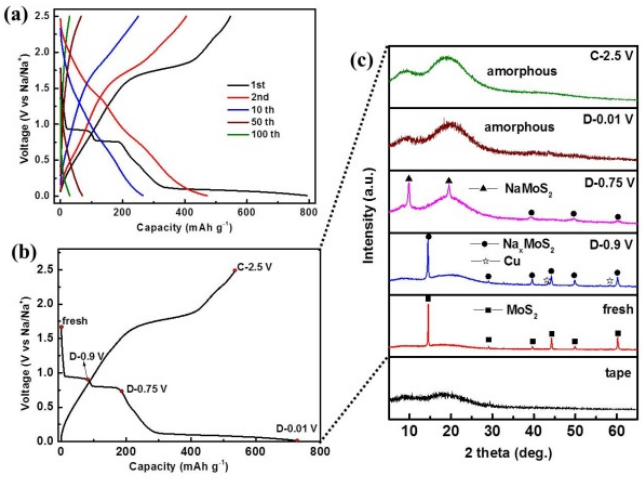

Figure 4. Mechanism of Na storage in MoS_2**:** (a) charge/discharge curves of C-MoS_2 in different cycles at 100 mA g^{-1}; (b) first charge/discharge curves at specified states at 10 mA g^{-1} and (c) corresponding ex-situ XRD patterns at a scan rate of 0.5° min^{-1} for different states of C-MoS_2 in 1.0 M $NaClO_4$ with PC.

amorphous nature of the product $Na_{x+1}MoS_2$ ($x \leq 3$). There is no doubt that a conversion reaction takes place during this process, so the theoretical capacity should be 668.0 mAh g^{-1} for the 4 Na^+ reactions. The capacity recorded is 720 mAh g^{-1}, with the exceed capacity mostly due to the formation of a SEI film. As the cells are discharged/charged at 0.01-2.5 V for 1 cycle, the diffraction pattern is amorphous, similar to that of the one discharged to 0.01 V, in agreement with the conversion reaction. The corresponding capacity is 535 mAh g^{-1}, which is equivalent to the desodiation of 3.2 Na^+ during the charge process, proving the irreversibility of the intercalation reaction (1 Na^+) and the high reversibility of the conversion reaction. In addition, two Cu peaks at 43.4° and 58.4° can be observed in the XRD patterns, an impurity arises from the Cu current collector. Based on the ex-situ XRD analysis, the sodium storage mechanism of MoS_2 in sodium ion batteries can be summarized as follows:

1st discharge process:

1st plateau: intercalation reaction

$$MoS_2 + 0.5\ Na^+ + 0.5e^- \longrightarrow Na_{0.5}MoS_2 \quad (1)$$

2nd plateau: intercalation reaction

$$Na_{0.5}MoS_2 + 0.5\ Na^+ + 0.5e^- \longrightarrow NaMoS_2 \quad (2)$$

3rd plateau: conversion reaction

$$NaMoS_2 + xNa^+ + xe^- \longrightarrow 2\ Na_{x+1}MoS_2\ (x \leq 3) \quad (3)$$

1st charge process: conversion reaction

$$Na_{x+1}MoS_2 \longrightarrow Na_{x-2}MoS_2 + 3\ Na^+ + 3e^- \quad (4)$$

Subsequent cycles: conversion reaction

$$Na_{x-2}MoS_2 + yNa \underset{\text{Charge}}{\overset{\text{Discharge}}{\longleftrightarrow}} Na_{x+y-2}MoS_2\ (y \leq 3) \quad (5)$$

As for the sodium-ion pseudocapacitors, the occurred reaction can be represented by:

$$Na_nMoS_2\ (n \leq 3) \leftrightarrows Na_{n-m}MoS_2 + mNa^+ + me^-(m<n) \quad (6)$$

The Na doped MoS_2 (Na_nMoS_2) can provide more sodium ions for this system and ensure the conversion reaction take place in the following cycles. On the other hand, the conversion reaction is highly reversible, and thus able to maintain long cycling life with good capacitance retention. In addition, the graphene matrix plays a key role in capacity/capacitance improvement in both systems, which can adsorb and desorb Na ions reversibly due to its large surface area and good electrical conductivity.

Conclusions

The graphene-like MoS_2/G composite was assessed with respect to its feasibility for Na-ion batteries and pseudocapacitors. The electrode is capable of delivering a high capacity of ~400 mAh g^{-1} over 200 cycles. The low initial coulombic efficiency and ex-situ XRD results confirm that the MoS_2 and Na undergo an irreversible intercalation reaction during the first charge, followed by a highly reversible conversion reaction. Interestingly, the conversion reaction, with typical high capacity and voltage hysteresis, can be applied in advanced NIC systems. In contrast to the MoS_2/G based capacitor, the capacitance of the Na_nMoS_2/G capacitor is significantly enhanced by 7 to 17 times at different currents, which is ascribed to the transformation of conventional EDLCs into advanced sodium-ion pseudocapacitors, so that the battery-like faradic reaction can take place. Accordingly, we believe that MoS_2/G has great potential for Na storage due to its advantages of nanostructure and its reversible conversion reaction mechanism.

Experimental sections

Synthesis of MoS_2/G composite:

Expanded MoS_2 (E-MoS_2) dispersion was prepared from commercial MoS_2 (C-MoS_2) via an expanded lithiation method[38] and the graphene oxide dispersion was achieved by a modified Hummers' method.[39] MoS_2/G composite (MoS_2/G) was synthesised by a facile hydrothermal method, followed by adding 60 ml E-MoS_2 aqueous dispersion (~3 mg/ml) and 30ml graphene oxides aqueous dispersion (~5 mg/ml). The obtained mixture was ultrasonicated for 3 min, and then loaded into Teflon-lined autoclaves, which were then sealed and maintained at 180 ^oC for 5 h. After cooling down to room temperature naturally, the black product was centrifuged, washed three times each with deionized water and absolute ethanol, and dried under vacuum at 80 ^oC overnight. The MoS_2/G was finally obtained after annealing treatment at 450 ^oC for 2 h and then at 800 ^oC for 2 h in a mixed 5 % H_2/Ar atmosphere.

Physical characterization:

The morphologies of the samples were investigated by field-emission scanning electron microscopy (FESEM; JEOL JSM-7500FA) and transmission electron microscopy (TEM, JEOL 2011, 200 keV). The XRD patterns were collected by powder X-ray diffraction (XRD; GBC MMA diffractometer) with Cu Kα radiation at a scan rate of 0.5° min^{-1} and 2° min^{-1}. Thermogravimetric analysis (TGA) was performed in air with a SETARAM Thermogravimetric Analyzer (France). Raman spectra were collected with a Jobin Yvon HR800 Ranman spectrometer with a 10 mW helium/neon laser at 632.8 nm excitation.

Electrochemical measurements:

The electrochemical measurements were conducted by assembling coin-type half cells in an argon-filled glove box. The slurry was prepared by fully mixing 80 wt % active materials, 10 wt % carbon black, and 10 wt. % polyvinylidene difluoride (PVdF) using a planetary mixer (KK-250S). Then, the obtained slurry was pasted on a copper film by a doctor blade in a thickness of 100 μm, which was followed by drying in a vacuum oven overnight at 80 °C. The working electrode was prepared by punching the electrode film into discs 0.97 cm in diameter. Sodium foils were cut using a surgical blade from sodium bulk to act as both reference and counter electrode. The electrodes were separated by a glass fiber separator. The electrolytes were 1.0 M $NaClO_4$ in 1:1 (weight ratio) propylene carbonate (PC) / ethylene carbonate (EC) with 5 wt% fluoroethylene carbonate (FEC) additive. The electrochemical performances were tested on a LAND Battery Tester.

Acknowledgments

This work was financially supported by the Australian Research Council through the following grants; Discovery Project DP100103909, Linkage Project LP120200432, and a LIEF Equipment Grant LE0237478. We would also like to acknowledge assistance of staff and use of facilities at the University of Wollongong Electron Microscopy Centre. We would especially like to acknowledge Dr. Tania Silver for critical reading of the manuscript.

Keywords: sodium battery • expanded MoS_2 • MoS_2/graphene composite • hydrothermal

[1] B. Dunn, H. Kamath, J. M. Tarascon, *Science* **2011,** *334* (6058), 928-35.
[2] M. Armand, J. M. Tarascon, *Nature* **2008,** *451* (7179), 652-657.
[3] M. Dubois, D. Billaud, *J. Solid State Chem.* **1996,** *127* (1), 123-125.
[4] J. Barker, R. K. B. Gover, P. Burns, A. J. Bryan, *Electrochem.Solid-State Lett.* **2006,** *9* (4), A190- A192.
[5] Y. Cao, L. Xiao, W. Wang, D. Choi, Z. Nie, J. Yu, L. V. Saraf, Z. Yang, J. Liu, *Adv. Mater.* **2011,** *23* (28), 3155-3160.
[6] R. Berthelot, D. Carlier, C. Delmas, *Nat. Materi.* **2010,** *10* (1), 74-80.
[7] D. Kim, S.-H. Kang, M. Slater, S. Rood, J. T. Vaughey, N. Karan, M. Balasubramanian, C. S. Johnson, *Adv. Energy Mater.* **2011,** *1* (3), 333-336.
[8] T. Kobayashi, Y. Kobayashi, M. Tabuchi, K. Shono, Y. Ohno, Y. Mita, H. Miyashiro, *ACS Appl. Mater. Interfaces* **2013,** *5* (23), 12387-12393.
[9] W. Deng, X. Liang, X. Wu, J. Qian, Y. Cao, X. Ai, J. Feng, H. Yang, *Sci. Rep.* **2013,** *3*, 2671.
[10] L. M. Zhu, Y. F. Shen, M. Y. Sun, J. F. Qian, Y. L. Cao, X. P. Ai, H. X. Yang, *Chem. Commun.* **2013,** *49* (97), 11370-11372.
[11] B. L. Ellis, W. R. M. Makahnouk, Y. Makimura, K. Toghill, L. F. Nazar, *Nat. Mater.* **2007,** *6* (10), 749-753.
[12] J. Zhao, J. He, X. Ding, J. Zhou, Y. Ma, S. Wu, R. Huang, *J. Power Sources* **2010,** *195* (19), 6854-6859.
[13] H. Kim, I. Park, D.-H. Seo, S. Lee, S.-W. Kim, W. J. Kwon, Y.-U. Park, C. S. Kim, S. Jeon, K. Kang, *J. Ame. Chem. Soc.* **2012,** *134* (25), 10369-10372.
[14] Z. Jian, L. Zhao, H. Pan, Y.-S. Hu, H. Li, W. Chen, L. Chen, *Electrochem. Commun.* **2012,** *14*, 86-89.
[15] Z. Jian, W. Han, X. Lu, H. Yang, Y.-S. Hu, J. Zhou, Z. Zhou, J. Li, W. Chen, D. Chen, *Adv. Energy Mater.* **2013,** *3*, 156-160.
[16] D. Stevens, J. Dahn, *J. Electrochem. Soc.* **2000,** *147* (4), 1271-1273.
[17] S. Komaba, W. Murata, T. Ishikawa, N. Yabuuchi, T. Ozeki, T. Nakayama, A. Ogata, K. Gotoh, K. Fujiwara, *Adv. Funct. Mater.***2011,** *21* (20), 3859-3867.
[18] Y.-X. Wang, S.-L. Chou, H.-K. Liu, S.-X. Dou, *Carbon* **2013,** *57* (0), 202-208.
[19] L. Xiao, Y. Cao, J. Xiao, W. Wang, L. Kovarik, Z. Nie, J. Liu, *Chem. Commun.* **2012,** *48* (27), 3321-3323.
[20] Y.-X. Wang, Y.-G. Lim, M.-S. Park, S.-L. Chou, J. H. Kim, H.-K. Liu, S.-X. Dou, Y.-J. Kim, *J. Mater.Chem. A* **2014,** *2* (2), 529-534.
[21] Y. Denis, P. V. Prikhodchenko, C. W. Mason, S. K. Batabyal, J. Gun, S. Sladkevich, A. G. Medvedev, O. Lev, *Nat. commun.***2013,** *4*.
[22] D. W. Su, H. J. Ahn, G. X. Wang, *Chem.Commun.***2013,** *49* (30), 3131-3133.
[23] H. Pan, X. Lu, X. Yu, Y.-S. Hu, H. Li, X.-Q. Yang, L.Chen, *Adv. Energy Mater.* **2013,** *3,* 1186-94.
[24] J. F. Qian, X. Y. Wu, Y. L. Cao, X. P. Ai, H. X. Yang, *Angew. Chem.* **2013,** *52* (17), 4633-4636.
[25] W.-J. Li, S.-L.Chou, J.-Z. Wang, H.-K. Liu, S.-X. Dou, *Nano Lett.* **2013,** *13* (11), 5480-5484.
[26] P. Simon, Y. Gogotsi, *Nat. Mater.* **2008,** *7* (11), 845-854.
[27] M. D. Stoller, S. Park, Y. Zhu, J. An, R. S. Ruoff, *Nano Lett.* **2008,** *8* (10), 3498-3502.
[28] K. Kuratani, M. Yao, H. Senoh, N. Takeichi, T. Sakai, T. Kiyobayashi, *Electrochim. Acta* **2012,** *76*, 320-325.
[29] Z. Chen, V. Augustyn, X. Jia, Q. Xiao, B. Dunn, Y. Lu, *Acs Nano* **2012,** *6* (5), 4319-4327.
[30] L. Ye, C. Wu, W. Guo, Y. Xie, *Chem.Comm.***2006,** (45), 4738-4740.
[31] S. K. Park, S. H. Yu, S. Woo, B. Quan, D. C. Lee, M. K. Kim, Y. E. Sung, Y. Piao, *Dalton Trans.* **2013,** *42* (7), 2399- 2405.
[32] J. Z. Wang, L. Lu, M. Lotya, J. N. Coleman, S. L. Chou, H. K. Liu, A. I. Minett, J. Chen, *Adv. Energy Mater.* **2013,** *3* (6), 798-805.
[33] K. Chang, W. Chen, *Acs Nano* **2011,** *5* (6), 4720-4728.
[34] K. Chang, D. Geng, X. Li, J. Yang, Y. Tang, M. Cai, R. Li, X. Sun, *Adv. Energy Mater.* **2013,** *3* (7), 839-844.
[35] J. Park, J.-S. Kim, J.-W. Park, T.-H. Nam, K.-W. Kim, J.-H. Ahn, G. Wang, H.-J. Ahn, *Electrochim. Acta* **2013,** *92*, 427-432.
[36] L. David, R. Bhandavat, G. Singh, *Acs Nano* **2014**.DOI:10.1021/nn406156b.
[37] R. H. Miwa, W. L. Scopel, *J. Physics: Condensed Matter* **2013,** *25* (44), 445301.
[38] R. Bissessur, P. K. Y. Liu, S. F. Scully, *Synthetic Metals* **2006,** *156* (16-17), 1023-1027.
[39] W. S. Hummers, R. E.Offeman, *J. Ame.Chem.Soc.***1958**, 80, 1339-1339.